Geochemical Perspectives Letters

Preservation of biosignatures in opal probed by infrared nanospectroscopy

S. Gouzy, V.T.H. Phan, L. Bejach, V. Vinogradoff, B. Rondeau, B. Chauviré, P. Beck, L. Flandinet, G. Franz, V. Khomenko, J. Carter

Supplementary Information

The Supplementary Information includes:

- Information on Samples and Deposits
- Details of the Analytical Conditions and both FTIR and AFM-IR Spectral Decomposition
- CHNS Elemental Analysis
- Tables S-1 to S-3
- Figures S-1 to S-4
- Supplementary Information References

Information on Samples and Deposits

Samples

The pink opal from Quincy was donated by the Muséum National d'Histoire Naturelle, France (MNHN_MIN_123.206). The specimen is a nodule a few centimetres long and wide with a limestone crust and an inhomogeneous bright pink distribution throughout its volume. The periphery of the opal sample appears pinker and most concentrated in a particular horizon, while the centre is paler. The Volyn black opal is from the museum collection of the National Academy of Sciences, Kyiv. The specimen is a few centimetres long and wide breccia of pegmatite cemented by opal. The opal represents 30% of the whole sample and the black body colour is homogeneous (Fig. S-1). Both opals are common opal-CT (without play-of-colour).

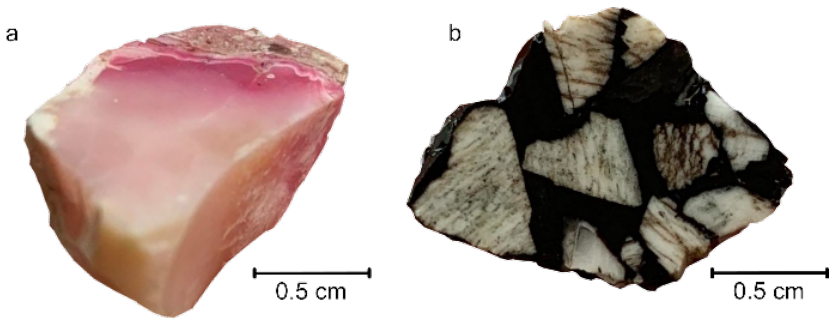

Figure S-1 photographs of the **(a)** Quincy pink opal sample and **(b)** the Volyn black opal sample.

Opal's insoluble residues were extracted by demineralization with HF/HCl acid attacks at IPAG (Grenoble, France) following to remove silicates and newly formed fluorides. This process involved the use of 41 mg of Quincy pink opal and 17 mg of Volyn black opal powders in a 4 mL solution under vortex agitation. The extraction protocol comprised the several stages: (1) Leaching with ultrapure water (Milli-Q water, 18.2 MΩ) and Toluene/Methanol (2/1 v/v) to extract soluble organic molecules; (2) Treatment with HCl 6N for 45 hours to remove carbonates, sulphides and other minerals, followed by ultrapure rinsing with ultrapure water twice overnight; (3) Acid treatment with HF (9M): HCl (4M) (2/1 v/v) for approximately 6h to eliminate the opal silica matric. (4) Rinsing with ultrapure water and HCl (3M)/H_3BO_3 (0.4M) for 24h to eliminate cations that could form insoluble fluorides; (5) Addition of dioxane for 5h, followed by rinsing with Toluene/Methanol (2/1 v/v) to remove any encapsulated free molecules; (6) Recovery of residue with methanol in the vial and evaporation under a fume hood. After each step, the sample was centrifuged for 5 mins at 10000 rpm, and the supernatant was discarded.

Deposits

The Volyn black opals form the cement of pegmatitic breccias in the Korosten pluton, dating from the end of the Palaeoproterozoic era (around 1800 to 1700 Myr). The age of fossils from this locality was recently estimated using the Ar-Ar laser-ablation method on muscovite (1,491±9 Myr), which is closely associated in a breccia with the black opal (Franz *et al.*, 2022a), and thus is the likely age of black opal. Buddingtonite however, also closely associated with muscovite and black opal, yielded an age spectrum, and the oldest obtained age of 563 ± 14 Myr was considered as the minimum age of the black opal. Direct dating of black opal with the $^{208}Pb/^{232}Th$ pair yielded ages around 1,500 ± 46 to 1,279 ± 35 Myr, but this remains to be further constrained, as the U-Th-Pb isotopic data indicate open-system behaviour (Franz *et al.*, 2022b). Thanks to this dating attempts, these opals are currently considered to be the oldest on Earth. The brownish-black colour of these opals is thought to be due to carbohydrates, which are probably kerite degradation products.

The Quincy pink opals correspond to siliceous accidents in the Berry lacustrine series (37.8 to 33.9 Myr), made up of marl and coarse detrital deposits on which different types of limestone over imposed: vermiculated, vacuolar, compact, pulverulent, breccias or silicified (Person *et al.*, 1994). This entire sedimentary sequence is thought to have formed as a result of the gradual drying up of residual shallow lakes separated by marshy soils that were also in the process of drying up, during an intense arid episode. The pink color has been observed and studied on other phases than opal, such as sepiolite, and after extraction was attributed to an assembly of several organic pigments, of which the major component (75%) is *2,8di-isopropyl-peri-xanthenoxanthene-4, l0-quinone* (Prowse *et al.*, 1991).

Details of the Analytical Conditions and both FTIR and AFM-IR Spectral Decomposition

Details of the Analytical Conditions

FTIR. The samples underwent initial preparation through grinding to 200 microns in ultrapure water to prevent organic contamination. Subsequently, they were polished on both sides for analysis using FTIR. Analysis were conducted using a Thermo-Nicolet FTIR 5700 spectrometer with a spectral resolution of 2 cm^{-1}, combined with a Thermo-Nicolet Continuμm microscope with a 200 x 200 μm beam size, located at LPG (Nantes, France). FTIR absorption spectra were acquired in the range 400 to 4000 cm^{-1} with an average repetition between 100 and 500 scans. The reference spectrum was taken at the beginning and end of each session (half a day) and every 3 samples.

Before analysis, the samples were stored in an oven at 50°C for 24 hours to prevent water absorption caused by ambient humidity. They were then placed inside an enclosure and exposed to a flow of dry compressed air during all the analysis. This procedure limits the contribution of atmospheric water during the analysis.

AFM-IR is a recent technique that combines the atomic force microscopy technology with infrared spectroscopy. The pulse and tuneable IR source locally heats the sample surface, inducing a thermal expansion that is directly proportional to the infrared absorption of the analysed sample. AFM-IR allows the acquisition of infrared maps at a fixed wavenumber, or local spectra covering the entire range of wavenumbers. Since the lateral resolution of the technique depends on the tip's radius of curvature (~10 nm), this provides access to the spatial distribution of organic matter within a crystalline matrix.

AFM-IR analysis were conducted using a nanoIR3s system at IPAG (Grenoble, France). Infrared images and absorption spectra were obtained at locations of interest. This setup features an AFM probe for topographical imaging and IR absorption measurement via photo-thermal expansion (Dazzi and Prater, 2017). The system uses an APE Carmina laser for mid-IR excitation (2000 to 600 cm^{-1}) and a Firefly IR laser for higher wavenumbers (3800 – 2700 cm^{-1}). Spectroscopy and imaging were performed in contact mode (CM) and tapping IR mode (TM). Prior to data collection, laser alignment and reference signal recording were conducted. AFM-IR images were captured using TM with laser power at 25 – 40 % and pulse rate at 340 - 400 kHz, optimized for minimal structural alteration. Various wavenumbers were targeted with the APE Mid-IR source operating in taping mode between 600 and 2000 cm^{-1}, including carbonyl (C=O) stretching (1720 cm^{-1}), sp^2 aromatic (C=C) (1600 cm^{-1}), CH_2 bending (1450 cm^{-1}), and silicate (Si-O) stretching (1100 cm^{-1}). The Firefly IR source operating in contact mode was employed to furnish both maps and spectra in the range of 3800-2700 cm^{-1} for comparison with conventional FTIR analysis, highlighting -OH stretching (3500 – 3700 cm^{-1}) and various -CH stretching bands (e.g. $-CH_3$ asymmetric stretch (2960 cm^{-1}); $-CH_2$ asymmetric stretch (2930 cm^{-1}); $-CH_2$ symmetric stretch (2860 cm^{-1}). Composite RGB colour images were generated for spatial component visualization using Analysis Studio software for Firefly TM data, and with realignment to correct for thermal drifts. Scan parameters included a speed of 0.1 Hz and varying scan sizes depending on region of interest (ROI) dimensions. The method has been described more detail in Phan *et al.* (2022, 2023).

Additionally, spectra were acquired with a spectral resolution of 4 cm^{-1}. Three spectra were systematically co-averaged for the APE, and five spectra for the FireFly. The AFM-IR analyses were

conducted using a semi-tapping gold-coated cantilever model PR-EX-TnIR-A-10 (resonance frequency: 75 ±15 kHz, spring constant: 1-7 $N.m^{-1}$), which allows for both contact and tapping AFM-IR modes.

Prior to analysis, the samples were ground into a powder and compressed between two diamond windows to create thin, flat samples (1-5 µm thick, with a typical area of 100 µm x 100 µm). To avoid interference and minimize beam intensity loss during transmission mode measurements, one of the windows was removed. This sample preparation reduced scattering artifact.

The following diagram (Fig S-2) provides an explanation of the interpretation of the results of the CH_2 AFM-IR signal study.

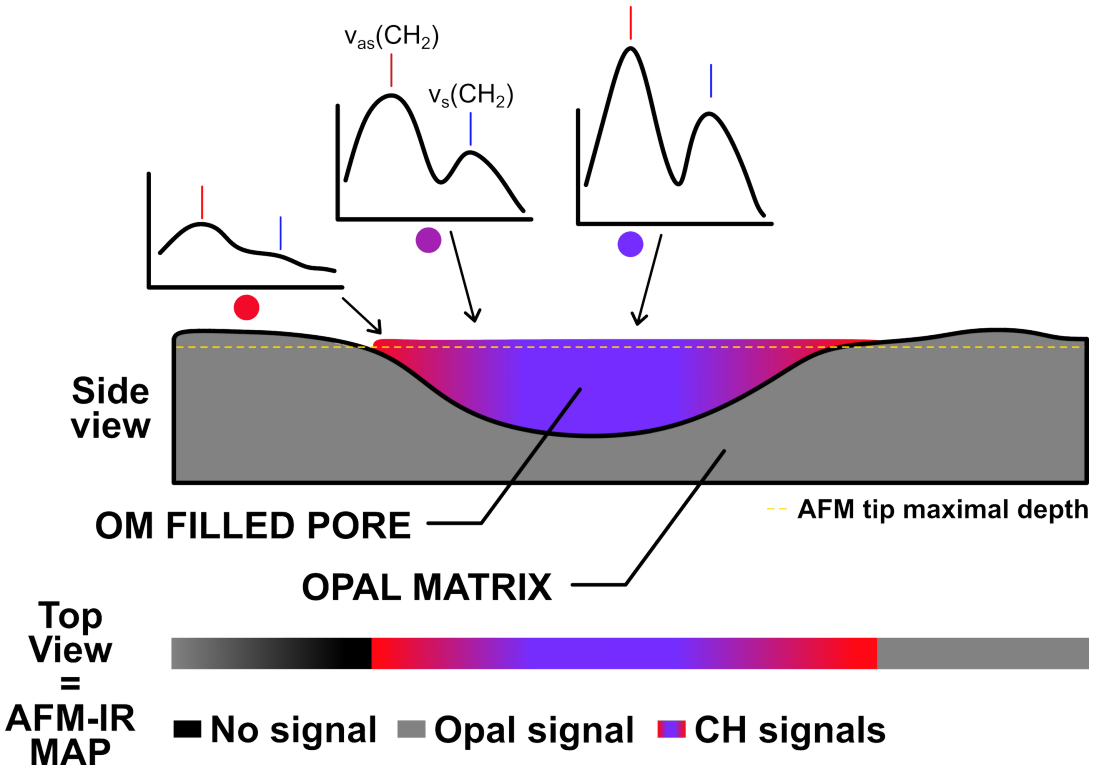

Figure S-1 Simplified schematic diagram of the morphology information obtained by OM signature of vas(CH_2) (red) and vs(CH_2) (blue).

FTIR And AFM-IR Spectral Decomposition

CH_2/CH_3 ratio by decomposition of FTIR spectra: branching and length of aliphatic chains. The FTIR absorption spectra presented in the Letter shows the characteristic bands of aliphatic C-Hx vibrations: for Quincy pink opal (Qy_2 and 3) and $\nu_s(CH_2)$ as well as $\nu_{as}(CH_2)$ for Volyn black opal (Vo_1, 2 and 3). These bands, although of low intensity, have been shown to be useful for assessing the chain length and degree of branching of aliphatic structures in MO (Lin and Ritz, 1993; Marshall *et al.*, 2005; Igisu *et al.*, 2009; Clodoré *et al.*, 2024). In particular, preliminary work by Lin and Ritz (1993) on macerals showed that the carbon number of n-alkanes and the ratio of CH_2/CH_3 band intensities (areas) in their IR spectra were correlated. As the carbon number (n) increases, so does the CH_2/CH_3 intensity ratio. Precise examination of this region by spectral decomposition therefore tends to provide valuable information about the nature of the OM contained in the samples.

The FTIR spectra were decomposed using Origin Pro 8 software (https://www.originlab.com/origin). For each spectrum, a baseline was applied between 2700 and 3000 cm^{-1} following the method of Orthous-Daunay *et al*. (2013). The parameters and methodology used are based on those of Lin and Ritz (1993) and Orthous-Daunay *et al*. (2013) with, in some cases, a few modifications based on observation of the spectra. Five components were defined in this spectral treatment and modelled by Gaussians: $\nu_s(CH_2)$ (2855 cm^{-1}), $\nu_s(CH_3)$ (2880 cm^{-1}), $\nu(CH)$ (2890 cm^{-1}), $\nu_{as}(CH_2)$ (2930 cm^{-1}) and $\nu_{as}(CH_3)$ (2965 cm^{-1}). Prior to each measurement presented in Figure 1c, f and Table S-1, a statistical fitting procedure was undertaken on one spectrum of each sample (Qy_3, Vo_2) in order to establish the best fitting parameters to be applied systematically to all the opal spectra, independently from the sample as we expect identical OM bonding behaviour. For this, we compared ten decomposition solutions provided by the Origin Pro 8 software computed with the same entry parameters for each spectrum. After that, a final decomposition were performed with each of the positions first manually placed on the associated precise band position (Colthup, 1950) and calibrated to have a degree of freedom of ± 10 cm-1 and a ± 20% authorized variation of the width at half maximum (FWHM) with respect to the calculated mean value. Five spectra, selected in advance on the basis of their band intensity, were decomposed using this method: Qy_2, Qy_3, VO_1, VO_2 and VO_3. Table S-1 shows the relative area of these five peaks (the sum being normalized to 100% - IntgP) and the CH_2/CH_3 ratio derived from the ratio of the area of the IR absorption peaks related to $\nu_{as}(CH_2)$ and $\nu_{as}(CH_3)$

Table S-1 Normalized FTIR intensity of the bands of interest and CH_2/CH_3 ratio.

Spectra	Area IntgP (%)					$\nu_{as}(CH_2)/\nu_{as}(CH_3)$
	$\nu_s(CH_2)$	$\nu_s(CH_3)$	$\nu(CH)$	$\nu_{as}(CH_2)$	$\nu_{as}(CH_3)$	
Vo_1	22.3	6.3	4.0	50.4	17.0	3
Vo_2	19.8	6.6	4.5	43.3	22.8	1.9
Vo_3	14.1	5.26	2.7	53.9	24.1	2.2
Qy_2	9.6	9.9	8.1	34.3	38.1	0.9
Qy_3	9.64	12.2	2.8	45.0	30.3	1.5

CO/C_{ar} ratio by decomposition of AFM-IR spectra: Relative abundance of functional groups. The AFM-IR spectra show the characteristic bands of symmetrical vibrations of CH_2 ($\delta(CH_2)$ - 1450 cm^{-1}); elongation of aromatic C=C (C_{ar} - 1620 cm^{-1}) and elongation of C=O carbonyl groups (CO - 1720 cm^{-1}). The intensity of these bands is directly proportional to the abundance of associated functional groups in the OM contained in the sample (Marshall *et al.*, 2005). Thus, the ratio of band intensities (areas) of carbonyl groups and aromatic C=C (CO/C_{ar}) can be used to assess their relative abundance in the OM composition. The slight shift between the C=C band at 1620 cm^{-1} and the vibrational frequency range of single aromatics (1580 to 1615 cm^{-1}) in the spectra of the two samples suggests that their OM has polyaromatic structures (Hudgins and Allamandola, 1997; Steemans *et al.*, 2010).

The AFM-IR spectra were also decomposed using Origin Pro 8 software (https://www.originlab.com/origin). The spectra obtained on the same sample (Quincy or Volyn) shows little variation in band shapes and intensity ratios. Based on this observation, we chose to decompose the most representative and least noisy signal for each sample: Vo_4_APE for Volyn black opal and Qy_3_APE for Quincy pink opal (Fig. S-3). Before decomposition, the signals were smoothed using the Savitzky-Golay algorithm (Savitzky and Golay, 1964) with a polynomial function of degree 3 and 40 window points. A baseline was performed between 1000 and 2000 cm^{-1}. Four components were defined in this spectral treatment and modelled by Gaussians around 1450, 1560, 1620 and 1720 cm^{-1}. The same statistical fitting procedure was used as for the FTIR spectra, resulting in a degree of freedom for the presented decomposition for each band position of ± 10 cm^{-1} with respect to the "optimal" wavelength number, and a variation of ±30 % in the FWHM with respect to the mean value obtained in the first step. Table 2-S shows the relative area of the four components (the sum being normalized to 100% - IntgP) and the CO/C_{ar} ratio.

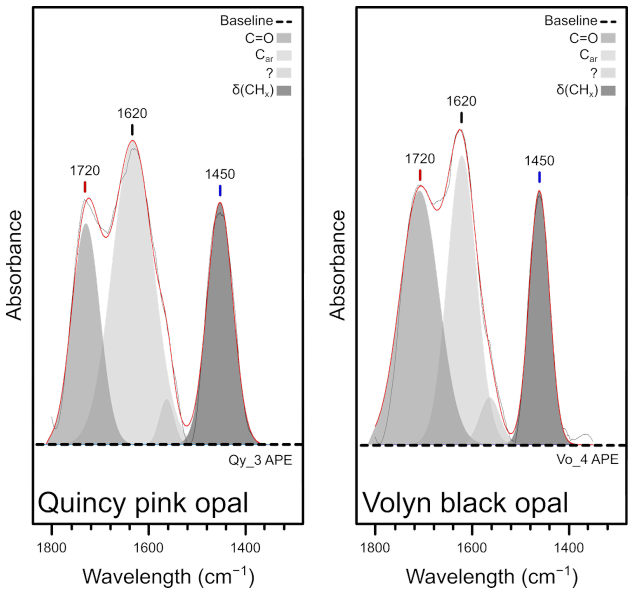

Figure S-2 Spectral decomposition of the most representative OM signals (b: Qy_3 APE; e: VO_4 APE)

Table S-2 Normalized AFM-IR intensity of the bands of interest and CO/Car ratio.

Spectra	Area IntgP (%)				CO/C_{ar}
	$\delta(CH_2)$	?	C_{ar}	CO	
Vo_4_APE	21.2	3.9	34.7	40.1	1.2
Qy_3_APE	24.5	2.6	48.8	24.2	0.5

CHNS Elemental Analysis

The CHNS measurements were carried out by the Elemental Analysis Department of the Spectropole de la Fédération des Sciences Chimiques Marseille on a Finnigan EA 1112 from Thermo Fisher. Each measurement was made twice on approximately 2-4 mg of sample, each time reduced to powder. No traces of nitrogen (N) or sulphur (S) were detected in either sample.

Table S-3 CHNS elemental analysis on the samples.

Measurements	Wt%			
	C	H	N	S
Qy_a	0.22	0.51	/	/
Qy_b	0.21	0.53	/	/
Vo_a	1.61	0.64	/	/
Vo_b	1.59	0.64	/	/
Instrumental Errors	±0.2 wt%	±0.1 wt%	±0.2 wt%	±0.2 wt%
Detection limits	0.05 wt%	0.1 wt%	0.01 wt%	0.01 wt%

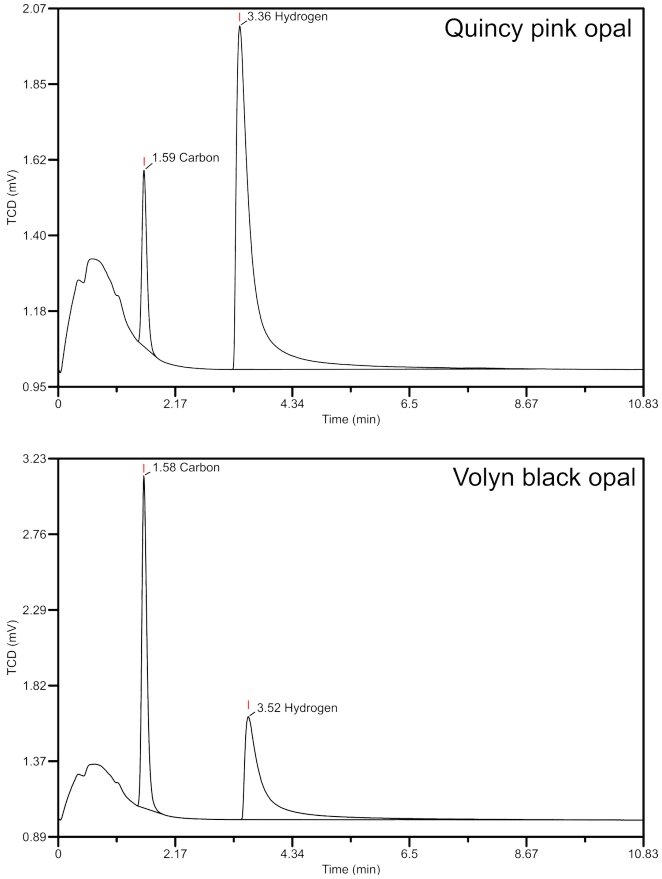

Figure S-3 CHNS elemental analysis spectra for both opal samples showing the detection of Hydrogen and Carbon.

Supplementary Information References

Clodoré, L., Foucher, F., Hickman-Lewis, K., Sorieul, S., Jouve, J., Réfrégiers, M., Collet, G., Petoud, S., Gratuze, B., Westall, F. (2024) Multi-Technique Characterization of 3.45 Ga Microfossils on Earth: A Key Approach to Detect Possible Traces of Life in Returned Samples from Mars. *Astrobiology* 24, 190–226. https://doi.org/10.1089/ast.2023.0089

Colthup, N.B. (1950) Spectra-Structure Correlations in the Infra-Red Region. *Journal of the Optical Society of America* 40, 397–400. https://doi.org/10.1364/JOSA.40.000397

Dazzi, A., Prater, C.B. (2017) AFM-IR: Technology and Applications in Nanoscale Infrared Spectroscopy and Chemical Imaging. *Chemical Reviews* 117, 5146–5173. https://doi.org/10.1021/acs.chemrev.6b00448

Franz, G., Lyckberg, P., Khomenko, V., Chournousenko, V., Schulz, H.-M., Mahlstedt, N., Wirth, R., Glodny, J., Gernert, U., Nissen, J. (2022a) Fossilization of Precambrian microfossils in the Volyn pegmatite, Ukraine. *Biogeosciences* 19, 1795–1811. https://doi.org/10.5194/bg-19-1795-2022

Franz, G., Sudo, M., Khomenko, V. (2022b) $^{40}Ar/^{39}Ar$ dating of a hydrothermal pegmatitic buddingtonite–muscovite assemblage from Volyn, Ukraine. *European Journal of Mineralogy* 34, 7–18. https://doi.org/10.5194/ejm-34-7-2022

Hudgins, D.M., Allamandola, L.J. (1997) Infrared Spectroscopy of Matrix-Isolated Polycyclic Aromatic Hydrocarbon Cations. 4. The Tetracyclic PAH Isomers Chrysene and 1,2-Benzanthracene. *The Journal of Physical Chemistry A* 101, 3472–3477. https://doi.org/10.1021/jp9609794

Igisu, M., Ueno, Y., Shimojima, M., Nakashima, S., Awramik, S.M., Ohta, H., Maruyama, S. (2009) Micro-FTIR spectroscopic signatures of Bacterial lipids in Proterozoic microfossils. *Precambrian Research* 173, 19–26. https://doi.org/10.1016/j.precamres.2009.03.006

Lin, R., Ritz, G.P. (1993) Studying individual macerals using i.r. microspectroscopy, and implications on oil versus gas/condensate proneness and "low-rank" generation. *Organic Geochemistry* 20, 695–706. https://doi.org/10.1016/0146-6380(93)90055-G

Marshall, C.P., Javaux, E.J., Knoll, A.H., Walter, M.R. (2005) Combined micro-Fourier transform infrared (FTIR) spectroscopy and micro-Raman spectroscopy of Proterozoic acritarchs: A new approach to Palaeobiology. *Precambrian Research* 138, 208–224. https://doi.org/10.1016/j.precamres.2005.05.006

Orthous-Daunay, F.-R., Quirico, E., Beck, P., Brissaud, O., Dartois, E., Pino, T., Schmitt, B. (2013) Mid-infrared study of the molecular structure variability of insoluble organic matter from primitive chondrites. *Icarus* 223, 534–543. https://doi.org/10.1016/j.icarus.2013.01.003

Person, A., Tourenq, J., Trochon, T. (1994) Sepiolite and silicifications as lacustrine paleoenvironment indicators in the upper part of the Cenozoic Berry limestones (Mehun-sur-Yevre basin, Cher, France). *Geobios* 27, 293–305. https://doi.org/10.1016/S0016-6995(94)80046-4

Phan, V.T.H., Rebois, R., Beck, P., Quirico, E., Bonal, L., Noguchi, T. (2022) Nanoscale mineralogy and organic structure in Orgueil (CI) and EET 92042 (CR) carbonaceous chondrites studied with AFM-IR spectroscopy. *Meteoritics & Planetary Science* 57, 3–21. https://doi.org/10.1111/maps.13773

Phan, V.T.H., Rebois, R., Beck, P., Quirico, E., Noguchi, T., Takase, M. (2023) Chemical functional characterization of immature and mature coals at the nanoscale by atomic force microscopy-based infrared spectroscopy (AFM-IR). *International Journal of Coal Geology* 267, 104196. https://doi.org/10.1016/j.coal.2023.104196

Prowse, W.G., Arnot, K.I., Recka, J.A., Thomson, R.H., Maxwell, J.R. (1991) The quincyte pigments: Fossil quinones in an eocene clay mineral. *Tetrahedron* 47, 1095–1108. https://doi.org/10.1016/S0040-4020(01)80947-9

Savitzky, A., Golay, M.J.E. (1964) Smoothing and Differentiation of Data by Simplified Least Squares Procedures. *Analytical Chemistry* 36, 1627–1639. https://doi.org/10.1021/ac60214a047

Steemans, P., Lepot, K., Marshall, C.P., Le Hérissé, A., Javaux, E.J. (2010) FTIR characterisation of the chemical composition of Silurian miospores (cryptospores and trilete spores) from Gotland, Sweden. *Review of Palaeobotany and Palynology* 162, 577–590. https://doi.org/10.1016/j.revpalbo.2010.07.006